Point defects in Ga$_2$O$_3$ Ⓕ

View Online   Export Citation   CrossMark

Matthew D. McCluskey[a] (ID)

AFFILIATIONS

Department of Physics and Astronomy, Washington State University, Pullman, Washington 99164-2814, USA

[a]**Author to whom correspondence should be addressed:** mattmcc@wsu.edu

ABSTRACT

In the field of high-power electronics, gallium oxide (Ga$_2$O$_3$) is attracting attention due to its wide bandgap and ability to be doped *n*-type. Point defects, including vacancies, impurities, and dopants, play important roles in optimizing device performance. This tutorial discusses the fundamental properties of point defects in monoclinic β-Ga$_2$O$_3$ and the methods employed to study them. Oxygen vacancies are deep donors that do not cause *n*-type conductivity but may compensate acceptors. Gallium vacancies are deep acceptors that can be partially passivated by hydrogen. Substitutional magnesium is a promising acceptor that produces a semi-insulating material and also forms a complex with hydrogen. Calcium and iron also have deep acceptor levels. Iridium deep donors are introduced into crystals grown from a melt in an Ir crucible. Other defects are introduced by irradiation with energetic particles such as neutrons or protons. In addition to altering the electronic properties, defects give rise to UV/visible emission bands in photoluminescence and cathodoluminescence spectra.

I. INTRODUCTION

Gallium oxide (Ga$_2$O$_3$) is emerging as an important wide-bandgap semiconductor for power electronics. To develop Ga$_2$O$_3$-based devices, dopants and defects must be understood and controlled. This tutorial gives an overview of point defects in this material and the methods used to investigate them. Ga$_2$O$_3$ has several crystal structures, and the most stable of which is the monoclinic β phase. All discussions in this tutorial refer to β-Ga$_2$O$_3$ unless stated otherwise.

There is a growing body of literature in this area, and only a representative sample is presented here. Interested readers are encouraged to consult review articles on materials and device issues by Higashiwaki *et al.*,[1] Stepanov *et al.*,[2] Pearton *et al.*,[3,4] and Galazka,[5] and a volume edited by Pearton *et al.*[6] A review of "ultrawide" bandgap semiconductors including Ga$_2$O$_3$ is given by Tsao *et al.*[7] Focused reviews are available on Ga$_2$O$_3$ bulk growth,[8] thin-film growth by sputtering,[9] defects,[10,11] and solar-blind photo-detectors.[12] General information about semiconductor defects, growth, and characterization of semiconductors can be found in Ref. 13, and more details about defect characterization are in a volume edited by Tuomisto.[14]

A. Historical background

The once-separate topics of gallium oxide and semiconductor devices can trace their origins to the same decade. The existence of Ga$_2$O$_3$ was predicted by Mendeleev in 1871, and the element Ga was discovered a few years later.[15] Around the same time, rectifying metal–semiconductor junctions were reported by Ferdinand Braun, a German high school teacher.[16] Braun found that the current–voltage relationship was nonlinear, violating Ohm's "law." The ability to pass current more freely in one direction than the other was important for radios. However, "crystal radios" were unreliable because defects in crystals were not well understood or controlled. In the 1920s, vacuum tubes became the preferred option, while semiconductors such as germanium were the subject of basic research.

Work on germanium proceeded through the 1940s, culminating with the revolutionary Bell Labs inventions of the point-contact transistor and bipolar transistor.[17] Silicon was seriously developed beginning in the 1950s. Its intrinsic advantages over germanium included its larger bandgap (1.1 vs 0.7 eV) and ease of forming an insulating native oxide layer (SiO$_2$). This latter property was important for metal–oxide–semiconductor field effect transistors (MOSFETs) and integrated circuits.[18]

For widespread applications like computing, silicon is hard to beat. However, other applications require different levels of electrical power and voltage.[19] Low-power/low-voltage (<1 kW, <400 V) devices are common in consumer electronics. Mid-power/mid-voltage (1–100 kW, 400 V–1.2 kV) applications include photovoltaic inverters and uninterruptable power supplies. High-power/high-voltage (>1 MW, >1.2 kV) systems are found in wind turbines and smart

power grids. It is in the mid- to high-power space that Ga_2O_3 could make a major contribution. In particular, improving the efficiency of power devices is an important component of energy conservation.

B. Power electronics

An example of a Ga_2O_3 metal–semiconductor field effect transistor (MESFET) is shown in Fig. 1.[20] For this device, an n-type thin film was grown on a semi-insulating substrate. Free electrons travel from the source to the drain. When the gate is negatively biased (relative to the source), electrons are repelled and the depletion region under the gate widens. For sufficiently negative gate voltage, the depletion width equals the film width, and current is effectively zero. The gate, thus, acts as an "on/off" switch that allows or prohibits current to flow. Consider the "off" mode, where current is blocked. For a large source-drain voltage, the electric field in the depletion region can get very high. If the maximum electric field exceeds a critical value, E_c, *electrical breakdown* will occur and current will flow.

For a power transistor, it is important to have a large critical breakdown field. One mechanism for breakdown is *tunneling*. At high electric fields, the conduction band (CB) and valence band (VB) tilt steeply, and it is possible for an electron to tunnel from the VB straight into the CB.[21] In this way, current will flow even in a pure semiconductor. A second mechanism is *impact ionization*, where a carrier collides with an atom, generating an electron and a hole. These free carriers then cause additional impact ionization events, leading to avalanche breakdown.

C. Benefits of a wide bandgap

A large bandgap E_g has a strong tendency to reduce the generation of free carriers and hence raise the critical field E_c. Ga_2O_3, with its wide direct gap of 4.8 eV, has a distinct advantage in this regard. Empirically, for direct-gap semiconductors,[22]

$$E_c = 1.73 \times 10^5 E_g^{2.5}, \tag{1}$$

where E_c is in V/cm and E_g is in eV. By inserting $E_g = 4.8$ eV for Ga_2O_3, the above equation yields a predicted breakdown field of 8.7 MV/cm. This value is significantly higher than competitors such as GaN (3.5 MV/cm) and 4H-SiC (3.2 MV/cm). Experimentally, breakdown field strengths near 3.8 MV/cm in Ga_2O_3 MOSFETs were reported by Green *et al.*[23]
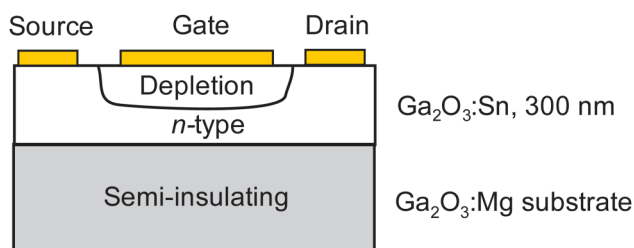

Source   Gate   Drain

Depletion

n-type Ga_2O_3:Sn, 300 nm

Semi-insulating Ga_2O_3:Mg substrate

FIG. 1. Schematic diagram of a Ga_2O_3 MESFET.[20]

Along with the critical field, an important design consideration is the power dissipated by the device. In the "on" state, the transistor should have low resistance R_{ON}. Baliga[24] proposed comparing devices with a fixed breakdown voltage. Given this constraint, a device made from a high-E_c material can be designed with a thin depletion region, which lowers R_{ON}. The Baliga figure of merit (BFOM) is defined as[25]

$$\text{BFOM} = \varepsilon \mu E_g^3, \tag{2}$$

where ε is the relative dielectric constant and μ is the carrier mobility. This metric points toward a large-gap semiconductor with good carrier mobility. Ga_2O_3 satisfies both of these criteria, with a bandgap of 4.8 eV and free-electron mobility of $\sim$100 cm^2/V s at room temperature.[26]

II. BASIC PROPERTIES

A. Crystal structure

β-Ga_2O_3 has a monoclinic crystal structure, denoted as $C2/m$.[27] The unit cell is shown in Fig. 2, where $\mathbf{a} \perp \mathbf{c}$, $\mathbf{b} \perp \mathbf{c}$, and the angle between $\mathbf{a}$ and $\mathbf{c}$ axes is 104°.[28] The lattice parameters are
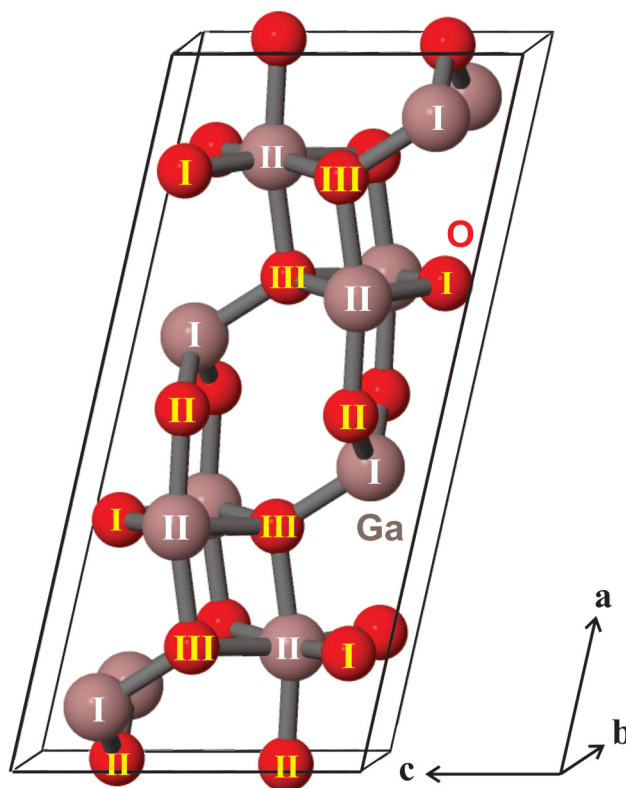

FIG. 2. Crystal structure of monoclinic β-Ga_2O_3. Some of the bonds, which extend to atoms in neighboring unit cells, are not shown. Figure made using a #3Dview from Ahman *et al.*, Acta Cryst. C **52**, 1336 (1996). Copyright 1996 @IUCr.

$a = 12.2$ Å, $b = 3.04$ Å, and $c = 5.80$ Å. There are two distinct Ga sites, labeled Ga(I) and Ga(II). The Ga(I) atoms are bonded to four neighboring O atoms in a (roughly) tetrahedral arrangement. The Ga(II) atoms are in an octahedral environment and bind to six neighboring O atoms. (Some of the bonds, which extend to atoms in neighboring unit cells, are not shown in Fig. 2.) The O atoms have three distinct sites: O(I) and O(II) bind to three Ga atoms while O(III) binds to four Ga atoms. There are four atoms of each type, for a total of $4 \times 5 = 20$ atoms in the unit cell (Fig. 2). The Ga–O bond lengths range from 1.8 to 2.1 Å.

B. Band structure

First-principles calculations show the conduction-band minimum (CBM) at the Brillouin zone center and a fairly flat VB (Fig. 3).[29,30] Quasiparticle (GW) calculations indicate a direct bandgap of 4.8 eV and indirect bandgap that is ∼0.1 eV lower.[31] This wide gap is key to its potential as a material for power electronics and has also been exploited for solar-blind detectors.[32] The bandgap can be estimated by measuring the transmission of light through the sample. Photon energies above the gap are able to excite an electron from the VB to the CB, leading to strong absorption. Optical transmission experiments show a room temperature bandgap absorption threshold near 4.8 eV (260 nm) or 4.5 eV (275 nm) for light polarized along the **b** or **c** axis, respectively.[33,34] This anisotropy has been explained in terms of selection rules for the VB-to-CB transition.[35,36] A detailed model of the absorption features is given in Ref. 37. In this paper, the bandgap is taken to be 4.8 eV.

C. Free carriers

Electronic transport has been investigated with the *Hall effect* and other electrical characterization methods.[38] For the Hall effect in the Van der Pauw geometry, four electrical contacts are placed on the sample on the corners of a square (Fig. 4). Current is sent through one pair of contacts while voltage is measured across the other pair. A magnetic field is applied perpendicular to the square.
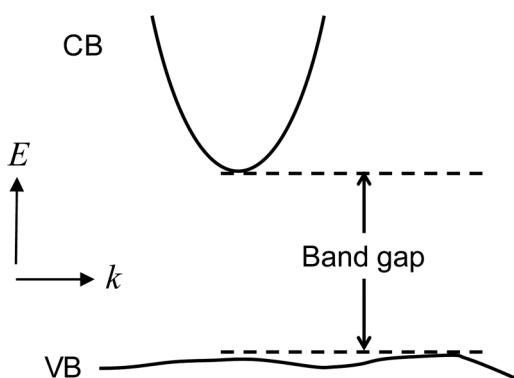
FIG. 3. Simplified band structure of Ga_2O_3. The minimum in the CB occurs at the zone center ($k = 0$). The indirect bandgap is shown. After A. Ratnaparkhe and W. R. L. Lambrecht, Appl. Phys. Lett. **110**, 132103 (2017).
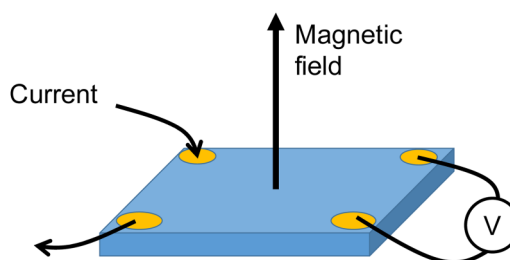
FIG. 4. Hall effect experiment in the Van der Pauw geometry. Current flows through two contacts and the voltage is measured across the other two. A magnetic field is applied perpendicular to the sample.

By measuring different contact-pair combinations, with and without a magnetic field, one can obtain the free-carrier mobility, density, and type (electrons or holes). Unintentionally doped Ga_2O_3 is generally *n*-type with electron mobilities around $100 \, cm^2/V \, s$.[39] First-principles calculations[40,41] indicate that phonon scattering is the primary limiting factor for room-temperature electron mobility ($<200 \, cm^2/V \, s$).

Free electrons lead to *IR absorption* and a *Burstein–Moss shift* of the optical bandgap. IR absorption is due to the electric field of the IR radiation accelerating electrons, i.e., Drude absorption. The Burstein–Moss shift occurs when there is a high density of electrons such that the Fermi level lies within the CB. For Ga_2O_3 with a high free-electron density of $10^{20} \, cm^{-3}$, the Fermi level is 0.2 eV above the CBM.[42] Because the states are filled up to the Fermi level, the VB-to-CB transition shifts to higher energy. The electron effective mass, calculated from the curvature of the CB, is $0.28 \, m$ for low doping and $0.36 \, m$ at high electron density, where m is the fundamental electron mass.

D. Growth

In contrast to nitride semiconductors, β-Ga_2O_3 bulk single crystals can be grown from the melt without the need for extreme pressures. With the *Czochralski* (CZ) method, Ga_2O_3 powder is melted in a heated iridium (Ir) crucible.[43] A seed crystal is dipped into the melt and raised slowly, drawing up the melt, which cools and crystallizes (Fig. 5). The seed and/or crucible are rotated to promote the growth of a symmetric, cylindrical ingot. Growth occurs in a mixture of CO_2 and O_2 in order to provide an optimal oxygen partial pressure that prevents decomposition. CZ-grown Ga_2O_3 typically contains Ir, Fe, and Si impurities, and Ga vacancies. A related technique, *edge-defined film-fed growth* (EFG), uses a die with a slit.[44] When the die is dipped into the melt, a liquid Ga_2O_3 film is drawn up through the slit by capillary action, where it cools and crystallizes. The ingot's shape is defined by the shape of the slit.

In *vertical Bridgman* growth, the crucible and starting powder are in a thermal gradient where temperature increases as a function of height. The crucible is lowered such that the solid–liquid interface moves upward slowly, resulting in crystal growth. Ga_2O_3 grown in a Pt–Rh crucible in the ambient air contained Si, Pt, and
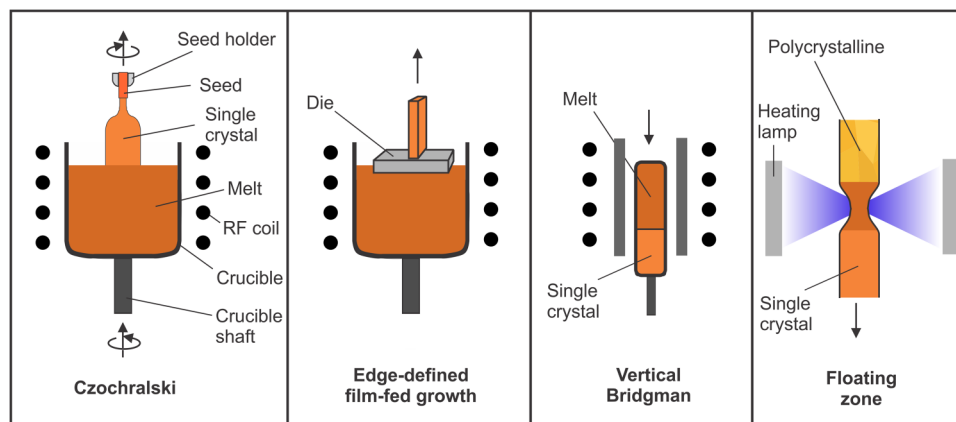
FIG. 5. Bulk crystal growth techniques.

Rh impurities at the 1–10 ppm level.[45] The *floating zone* technique starts with a polycrystalline rod, which is melted by halogen heating lamps. The rod is translated vertically so that the molten zone moves through the length of the rod, leaving behind single-crystal Ga_2O_3.[46] Crystals grown this way have free-electron densities of $\sim 10^{17}\,cm^{-3}$, likely due to Si impurities, similar to CZ-grown crystals.

Ga_2O_3 thin films have been grown using a variety of methods. *Sputtering* is a relatively inexpensive technique that uses an Ar^+ plasma to dislodge, or sputter, atoms from a Ga_2O_3 target.[9] The plasma (Ar^+ ions and electrons) is created by a radio frequency (RF) power source. A magnetic field is typically applied in order to bend electrons into helical paths, which confines the electrons and makes them ionize many Ar atoms. The sputtered Ga and O atoms coat the substrate, forming a thin film. *Pulsed laser deposition* (PLD), which uses a high-intensity laser to ablate target atoms, has also been used.[47]

Sputtering and PLD generally do not yield *epitaxial* growth. Epitaxy is defined as the growth of a crystalline film on a crystalline substrate with well-defined atomic bonds between the film and the substrate.[48] Because single-crystal substrates can be grown, it is straightforward to grow Ga_2O_3 on Ga_2O_3 substrates. This is referred to as *homoepitaxy*. The growth of Ga_2O_3 on a different substrate, such as sapphire (Al_2O_3), is an example of *heteroepitaxy*.

Metalorganic chemical vapor deposition (MOCVD) is a preferred epitaxial growth technique. Typical starting molecules, or precursors, are trimethyl gallium (TMGa) and oxygen gas. The precursors are transported to the substrate by a carrier gas such as Ar, adsorb on the surface, and dissociate. The Ga and O atoms go to the proper sites by surface diffusion. During growth, the substrate is maintained at a temperature around 500–850 °C.[49] A similar technique, *halide vapor phase epitaxy* (HVPE), uses GaCl and oxygen as the precursors.[50] $SiCl_4$ or $SnCl_4$ can be used to dope with Si or Sn donors. HVPE has a fast growth rate, over $100\,\mu m/h$, making it attractive from an industrial point of view.

Finally, *molecular beam epitaxy* (MBE) is an ultrahigh-vacuum technique that enables atomic layer control. Thanks to the vacuum, atoms travel from the source to the substrate without colliding with each other. For Ga_2O_3 MBE growth, the gallium source is Ga evaporated from an oven (Knudson cell), and either oxygen plasma[51] or ozone[52] is used as the oxygen source. As the sources are turned "on" and "off," the film is grown layer by layer.

E. Point defects

A *point defect* is an imperfection that occurs at a specific location, or point, in a crystal. This is in contrast to an *extended defect*, which is not localized at a specific lattice site. A *dislocation*, for example, is a one-dimensional "line" defect. When there is an extra plane of atoms in the lattice, the edge of that plane is a line and is referred to as an edge dislocation. A *stacking fault*, where a plane of atoms is in the wrong sequence, is an example of a two-dimensional defect. Dislocations, stacking faults, and hollow nano-pipes have been observed in Ga_2O_3.[10,53–55]

Point defects in crystals fall into two categories: (1) *native* defects, which involve only the atoms of the host crystal, and (2) *extrinsic* defects, which involve impurity atoms. When an impurity is deliberately introduced into a semiconductor, it is referred to as a *dopant*. A *vacancy*, or missing atom, is a type of native defect. Oxygen and gallium vacancies are denoted as V_O and V_{Ga}, respectively. If an oxygen or gallium atom is not in its proper site, then it is a *self-interstitial* (O_i and Ga_i). Self-interstitials may be created when an energetic particle such as a proton knocks the atom out of its lattice site. However, there is limited experimental evidence for Ga or O interstitials under normal conditions.

A very important quantity is the defect *formation energy* (E^f). If the formation energy is low, then the sample may contain many defects. The concentration of such defects is given by

$$N = N_{sites}\exp(-E^f/k_B T), \qquad (3)$$

where N_{sites} is the concentration of available sites for the defect, k_B is Boltzmann's constant, and T is temperature in Kelvin.

Group IV elements such as Si or Sn substitute for a host Ga atom. These *donors* have one more valence electron than the group-III Ga. This extra electron can be thermally excited to the CB, making the crystal *n*-type. The energy required to excite the electron to the CB is the *donor binding energy*. Because the donor binding energy is only tens of meV, Si and Sn are referred to as *shallow*

donors. The group-II elements Mg and Ca also substitute for a host Ga. Because they have one fewer valence electron than Ga, they are *acceptors*. The energy required to excite an electron from the VB to the acceptor level is quite large; because of this, Mg and Ca are *deep acceptors*.

III. NATIVE DEFECTS

A. Oxygen vacancies

In oxide semiconductors, a missing oxygen atom, or oxygen vacancy (V_O), is hard to detect. Perhaps because of this elusiveness, oxygen vacancies often get blamed for unintentional *n*-type conductivity. Most of the information we have for V_O in Ga_2O_3 comes from density functional theory (DFT). This "first-principles" technique calculates quantities based on the electron density distribution and positions of the nuclei. Recently, *hybrid functionals* have been employed to obtain reasonably accurate energy levels and bandgaps.[56]

Let us look at the example of V_O. First, the total electron energy (potential plus kinetic) is calculated for the intrinsic semiconductor. All the bond lengths are allowed to vary, or *relax*, to minimize the energy. Then, an oxygen atom is removed and placed into a reservoir. In this reservoir, the oxygen's energy is given by the chemical potential μ_O. The formation energy is the energy difference between the material with one defect and material that is pure (intrinsic).

An additional factor to consider is the charge state q of the defect. If $q = 1$, the defect has given one electron to the electron reservoir, where the electron's energy is the Fermi energy E_F. If $q = 2$, then the defect donated two electrons. In general, the contribution to the formation energy due to charge state is qE_F. Taking everything into account, the formation energy is

$$E^f = E(Ga_2O_3{:}V_O) - E(Ga_2O_3) + \mu_O + qE_F, \qquad (4)$$

where $E(Ga_2O_3{:}V_O)$ and $E(Ga_2O_3)$ are the calculated energies for the defective and pure semiconductor, respectively. Energies are relative to the valence-band maximum (VBM).

The results of calculations by Varley *et al.*[57] are shown in Fig. 6 for the oxygen vacancy at three different sites (I, II, and III). From Eq. (4), the slope of E^f vs E_F equals the charge state q. When looking at a formation energy plot, one can infer the charge state from the slope of a line. The oxygen vacancy is an example of a *negative-U* defect, where the +1 charge state is unstable. When the Fermi energy is low, the energetically preferred charge state is $q = 2$. When the Fermi energy is high, the charge state is neutral ($q = 0$). In the literature, it is common to show only the charge state that has the lowest formation energy for a given Fermi energy.

The point where the lowest-energy state goes from $q = 2$ to 0 is shown as a horizontal line in an energy-level diagram (Fig. 6). Because this (0/2+) level is far from the CB, the defect is a *deep donor*. The amount of thermal energy required to promote an electron from the defect level to the CB is much greater than the room temperature. Therefore, oxygen vacancies cannot be responsible for *n*-type conductivity in Ga_2O_3. They can, however, *compensate* acceptors by donating their electrons. As acceptor doping increases, the Fermi level is pushed down toward the VB. This reduces the
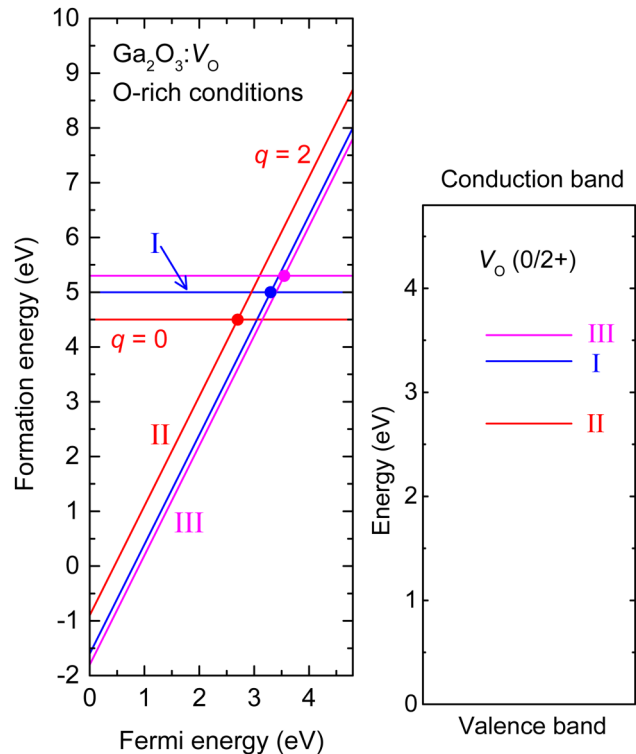

FIG. 6. Left: Formation energy for oxygen vacancy at O(I), O(II), and O(III) sites.[57] Right: Energy-level diagram showing the (0/2+) donor levels in the bandgap.

formation energy for oxygen vacancies. At some point, the formation energy gets small such that the Fermi level is prevented from going any lower.

Finally, note that the formation energy plotted in Fig. 6 is for O-rich conditions. This environment exists when the sample is in contact with O_2 gas. A sample in vacuum, hydrogen, or in contact with Ga would be in an O-poor (Ga-rich) environment. In that case, the chemical potential μ_O, and hence E^f, is lowered by ~3.5 eV.[57] The lower formation energy results in a higher V_O concentration [Eq. (3)].

B. Gallium vacancies

Gallium vacancies (V_{Ga}) are common defects in Ga_2O_3. Because Ga has three valence electrons, a missing Ga atom leaves behind three O dangling bonds that can accept electrons. V_{Ga}, therefore, acts as a triple acceptor. This is important because V_{Ga} can compensate donors, reducing free-electron concentration. Calculations show that the Ga(I) vacancy has a lower formation energy than Ga(II).[58,59]

The structure of V_{Ga} is unusual. Figure 7 shows a piece of the crystal structure (the middle portion of Fig. 2) with one Ga(I) removed. It is energetically favorable for a neighboring Ga(I) atom to leave its site and reside in the middle of the six-oxygen cage.
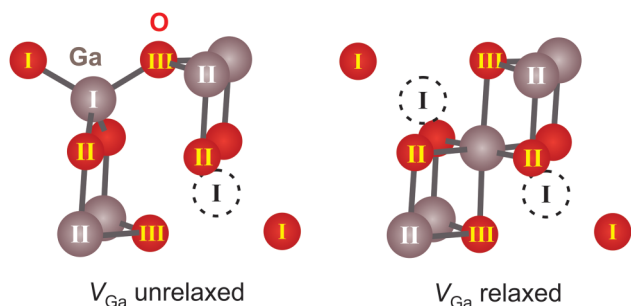
FIG. 7. Illustration of the gallium vacancy, where the relaxed model is the lowest-energy one. Missing Ga(I) atoms are indicated by dashed circles.

This *relaxation* process results in two "half vacancies" with a Ga atom in-between. In the figure, the displaced Ga atom is bonded to four O(II) and two O(III) atoms. It is also possible to have a vacancy where the displaced Ga atom binds to four O(II) and two O(I). A recent study used scanning transmission electron microscopy (STEM) to produce high-resolution images of a Ga_2O_3 sample.[60] The images showed a structure quite similar to Fig. 7 (V_{Ga} relaxed).

Electron paramagnetic resonance (EPR) is an excellent technique for characterizing defects that have unpaired spins. When a magnetic field is applied, the energies of spin-up and spin-down electrons split. A microwave source can excite a transition from down to up. In practice, the magnetic field is varied while the microwave frequency is fixed, and the derivative of the absorption spectrum is plotted (Fig. 8). For a spin-1/2 electron, the microwave excites a transition when

$$h\nu = \mu_B g B, \tag{5}$$

where $h\nu$ is the microwave photon energy, g is the Lande factor (~ 2 for a free electron), μ_B is the Bohr magneton, and B is the applied magnetic field. The exact value of g depends on the particular defect and the orientation of the field with respect to the crystal.

In an *n*-type sample, the gallium vacancy is fully occupied and has a charge $q = -3$, denoted V_{Ga}^{3-}. The electrons are paired, so there is no EPR signal. Kananen et al.[61] irradiated a sample with high-energy neutrons, creating vacancies and lowering the Fermi energy below the (2−/3−) level. This resulted in the V_{Ga}^{2-} defect, which has one unpaired spin ($S = 1/2$) located on one of the O(I) atoms near the vacancy. In a perfect crystal, O(I) has three Ga neighbors, but because of the vacancy it has only two. The EPR spectrum showed hyperfine splitting due to neighboring ^{69}Ga and ^{71}Ga nuclei, both of which have spins of $I = 3/2$ (Fig. 8). The authors also found evidence for V_{Ga}^{-}, which has two unpaired spins for a total spin of $S = 1$.[61]

Another method for detecting gallium vacancies is *positron annihilation*.[62] A positron, or anti-electron, is positively charged. When it annihilates an electron, two gamma rays are emitted. If a positron becomes trapped in a gallium vacancy, its lifetime increases because the electron density is low in the open volume of the vacancy. This increased lifetime allows one to estimate the concentration and type of vacancies. Also, the momenta of the electrons in the
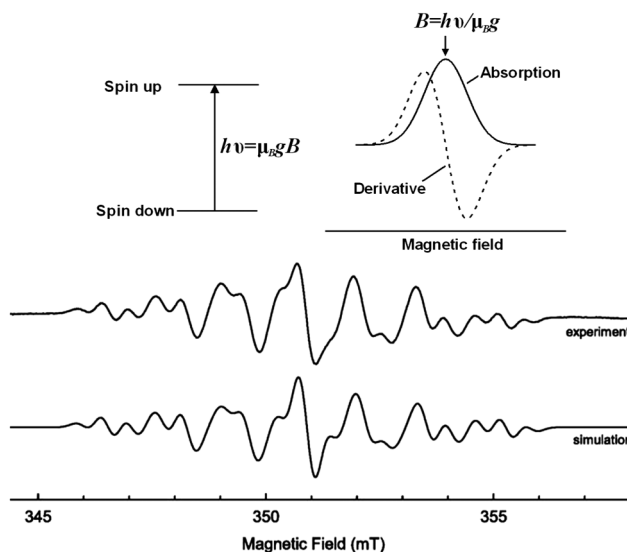

FIG. 8. Top: Illustration of an EPR transition and spectra. Bottom: Experimental and simulated EPR derivative spectra of gallium vacancies (V_{Ga}^{2-}). Splittings occur due to hyperfine interactions between the electron spin, localized on an O atom, and two neighboring Ga nuclear spins. Spectra reprinted with permission from Kananen *et al.*, Appl. Phys. Lett. **110**, 202104 (2017). Copyright 2017 AIP Publishing.[61]

vacancy are different than those in the pure crystal, which leads to subtle changes in the gamma-ray spectrum. Positron annihilation experiments have confirmed that V_{Ga} is a compensating acceptor in *n*-type Ga_2O_3.[63]

C. Hydrogenated gallium vacancies

As noted in Sec. III B, the gallium vacancy is a triple acceptor, i.e., it has three dangling bonds. A hydrogen atom can passivate an acceptor such as V_{Ga} by providing an electron and forming an O–H bond. The O–H bond-stretching vibrational mode is detected by *IR spectroscopy*.

In order to be "IR-active," a dipole moment must be induced by the vibrational motion. An IR-active mode results in a peak in the IR absorption spectrum. Classically, the absorption of light comes about because the electric field pushes and pulls the impurity atom. The electromagnetic energy goes into driving mechanical motion, resulting in a dip in the transmitted light intensity I at the vibrational frequency ν. Frequency is usually expressed as wavenumbers (cm^{-1}), which is defined as

$$\text{Wavenumber} \equiv 1/\lambda = \nu/c, \tag{6}$$

where λ is the wavelength of IR light and $c = 3.0 \times 10^{10}$ cm/s. IR spectra are typically plotted in absorbance units,

$$\text{Absorbance} = \log_{10}(I_0/I), \tag{7}$$

where I_0 is a reference spectrum that does not contain the defect. In this paper, IR spectra are for samples at low temperatures (5–12 K) unless stated otherwise.
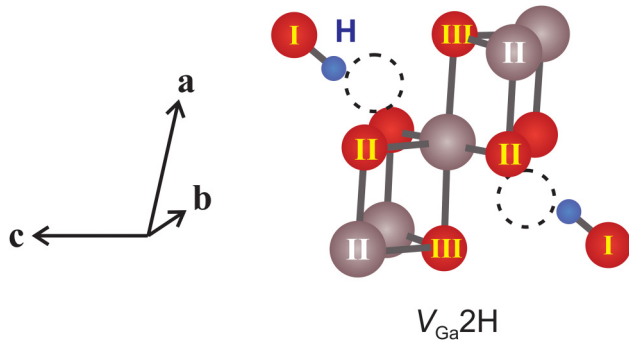
FIG. 9. Illustration of the hydrogenated gallium vacancy. Missing Ga(I) atoms are indicated by dashed circles.

When Ga_2O_3 is annealed in H_2 gas at temperatures above 800 °C, hydrogen forms a complex with V_{Ga}.[64] This complex, denoted as $V_{Ga}2H$, has two hydrogen atoms that form O–H bonds (Fig. 9). A simplified mass-spring model is shown in Fig. 10. When the H atoms oscillate together, a dipole moment is induced. This *asymmetric* vibrational mode absorbs IR light at a vibrational frequency of $3437\,cm^{-1}$. The *symmetric* mode, on the other hand, does not induce a net dipole moment, resulting in no IR absorption peak. The $3437\,cm^{-1}$ peak has polarization dependence. Light polarized along the **b** axis, [010], is perpendicular to the O–H bonds and, therefore, does not excite the vibrational mode (Fig. 10).

When hydrogen is replaced by deuterium, the heavier isotope results in a lower vibrational frequency. Deuterated samples form $V_{Ga}2D$ with a corresponding O–D line at $2546\,cm^{-1}$. Samples annealed in an H_2/D_2 mixture form $V_{Ga}2H$, $V_{Ga}2D$, and $V_{Ga}HD$ complexes. The latter complex gives rise to two new peaks corresponding to its O–H and O–D vibrations [Figs. 10(c) and 10(d)]. The appearance of these new peaks provides strong evidence that the defect has two hydrogen atoms.

As the sample is warmed from 5 K to room temperature, $V_{Ga}2H$ shifts to lower frequency by $-8\,cm^{-1}$.[65] This shift is due to interactions between O–H and neighboring atoms, which jiggle as the temperature increases. Along with a shift, the peak broadens. The broadening occurs because the random motion of the neighboring atoms interrupts the O–H oscillation, effectively reducing the vibrational lifetime.

IV. EXTRINSIC DEFECTS

A. Shallow donors

A substitutional single donor has one more valence electron than the atom it replaces. An example is silicon (Si_{Ga}), which has four valence electrons and substitutes for trivalent gallium. The extra electron orbits the positively charged Si_{Ga} impurity, analogous to the hydrogen atom. The amount of energy required to liberate the electron is called the *donor binding energy* and is estimated by the Bohr model,
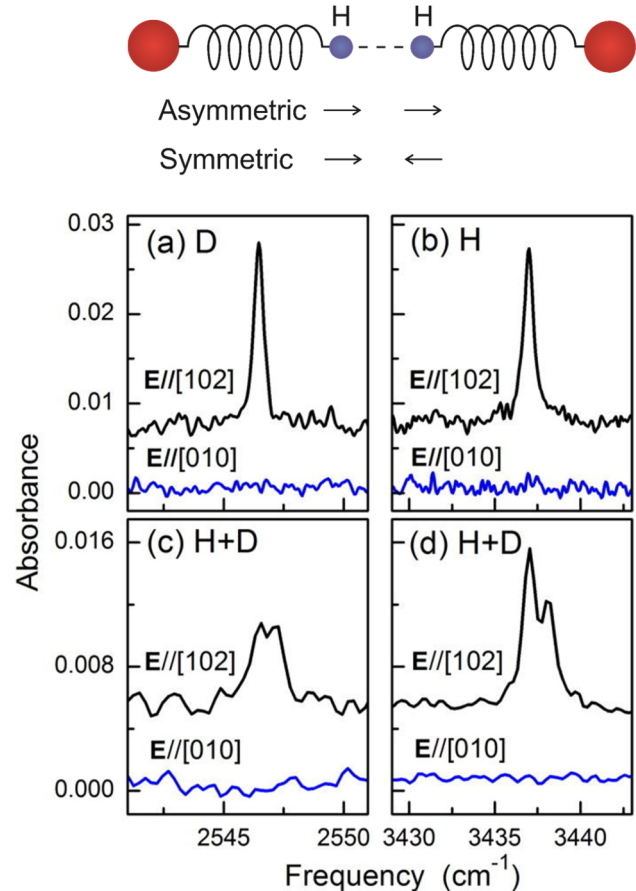
$$E_d = (13.6\,eV)(m^*/m)(1/\varepsilon^2), \qquad (8)$$

FIG. 10. IR transmission spectra of $V_{Ga}2H$ complexes. Samples with a mixture of H and D show new peaks that correspond to $V_{Ga}HD$ centers. IR light polarization along [010] is perpendicular to O–H bonds and is not absorbed. Spectra reprinted with permission from Weiser *et al.*, Appl. Phys. Lett. **112**, 232104 (2018). Copyright 2018 AIP Publishing.[64]

where $m^*/m \approx 0.28$ and the relative dielectric constant is $\varepsilon \approx 11$.[66] Inserting those values into Eq. (8) yields $E_d \approx 30\,meV$. On an energy-level diagram, the (0/+) donor level is depicted as a horizontal line E_d below the CBM (Fig. 11). Because the level is close to the CBM, it is referred to as a *shallow donor*. Shallow donors give rise to an EPR transition with $g \approx 1.96$.[67]

In addition to being a source of unintentional *n*-type conductivity in bulk Ga_2O_3,[68] deliberate Si doping can yield free-electron concentrations in the 10^{16}–$10^{18}\,cm^{-3}$ range.[69] Silicon doping has also been achieved during thin-film deposition[70] and by ion implantation.[71] The group-IV elements Ge and Sn have also been used to obtain *n*-type thin films.[72,73] Calculations indicate that Si and Ge prefer the Ga(I) site while Sn occupies the Ga(II) site.[57] Zirconium, a transition metal, acts as a shallow donor in bulk Ga_2O_3.[74] The neutral charge state (0) is typically denoted as Zr^{3+} because Zr^{3+} is neutral with respect to the trivalent Ga^{3+} atom that it replaces. The positive charge state (+) is labeled Zr^{4+}.
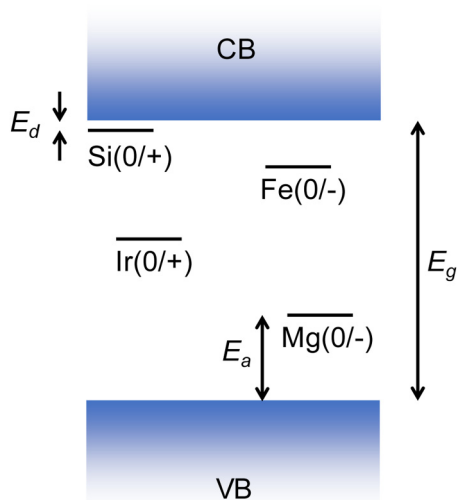
FIG. 11. Estimated energy levels for selected impurities in Ga_2O_3 (E_g = 4.8 eV). The hydrogenic (shallow) donor level is E_d = 30 meV, and the calculated Mg acceptor level is E_a = 1.0–1.5 eV. Theory and experiment place the Ir deep donor level 2.2–2.3 eV below the CBM. DLTS experiments indicate that the Fe acceptor level lies 0.8 eV below the CBM.

Hydrogen has two forms that are predicted to act as shallow donors, *interstitial* and *substitutional*.[57] Interstitial hydrogen (H_i) forms a bond with a host oxygen atom. Substitutional hydrogen (H_O) is essentially a proton inside an oxygen vacancy. While H_i should give rise to an O–H peak in the IR spectrum, H_O has a low vibrational frequency that lies in the two-phonon absorption spectrum, making it hard to detect. Evidence for hydrogen shallow donors was obtained indirectly by measuring an increase in free-carrier absorption after annealing in hydrogen.[75] The measurements further indicated that there is a reservoir of "hidden hydrogen" that releases hydrogen donors upon annealing in an inert gas.

B. Deep acceptors

A promising dopant for semi-insulating Ga_2O_3 is magnesium (Mg_{Ga}),[76,77] which sits on a Ga(II) site. Because Mg has two valence electrons, one fewer than Ga, it acts as an acceptor. The acceptor level is calculated to be deep, 1.0–1.5 eV above the VBM.[78,79] For neutral Mg, the hole is very localized, residing on an O(I) atom adjacent to Mg.[80] Ritter *et al.*[79] found that high concentrations of Mg (10^{18}–10^{19} cm^{-3}) can be incorporated in bulk crystals, enough to overwhelm compensating donors. This is great for the semi-insulating material, but *p*-type conductivity is not practical with such a deep acceptor. Indeed, substitutional acceptor dopants are all calculated to be deep.[81]

Hydrogen passivates Mg, forming a neutral MgH complex in samples annealed in hydrogen at 800 °C.[79] This center consists of an O–H bond oriented primarily along the **a** axis. IR absorption spectroscopy indicates a bond-stretching vibrational frequency of 3492 cm^{-1} (Fig. 12). The corresponding O–D mode is 2586 cm^{-1}. Samples annealed in hydrogen–deuterium mixtures show the O–H and O–D peaks, but no new peaks that might indicate multiple hydrogen atoms. Therefore, the MgH complex contains only one hydrogen. IR spectra taken with a polarizing filter show that the peak is strongest when **E**//**c** and zero when **E**//**b**. Hence, the O–H dipole is oriented in the *a*–*c* plane, consistent with calculations.

Resistance measurements with pressed indium contacts give a rough estimate of how acceptors affect the electrical properties. While nominally undoped Ga_2O_3 has a resistance of ~10 kΩ, Mg-doped samples have very high resistance (>100 GΩ). Ga_2O_3:Ca
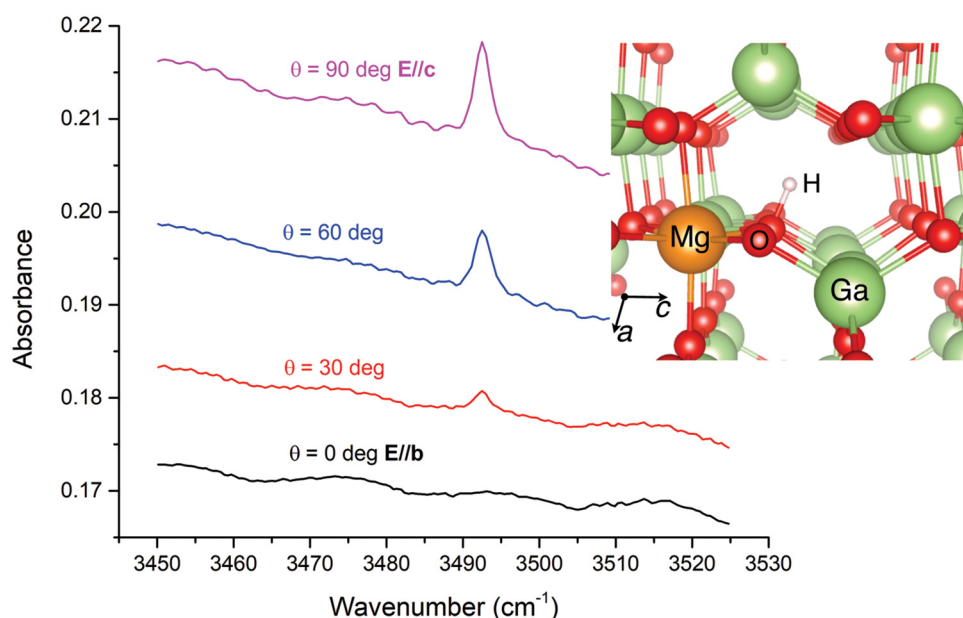
FIG. 12. Polarized IR transmission spectra of the MgH complex. The structure of the complex obtained from first-principles calculations is shown in the inset. Reprinted with permission from Ritter *et al.*, Appl. Phys. Lett. **113**, 052101 (2018). Copyright 2018 AIP Publishing.[79]

is *n*-type but has a higher resistance than an undoped material, ~10 MΩ, indicating that Ca acceptors partially compensate the donor impurities. Ga_2O_3:Ca annealed in hydrogen gives rise to an IR peak at 3441 cm^{-1}, attributed to an O–H bond-stretching mode of a CaH complex.[82] The corresponding O–D line has a frequency of 2558 cm^{-1}.

Deep-level transient spectroscopy (DLTS) has been used to study deep levels introduced by defects such as Fe, a common contaminant. DLTS is a technique that measures the rate at which a defect captures and releases free carriers. Consider a junction between metal and *n*-type Ga_2O_3. Assume that the donors are shallow such that they all give their electrons to the CB. In addition to shallow donors, the sample contains *electron traps*, which have deep levels in the upper portion of the bandgap. An applied reverse

FIG. 13. Illustration of the DLTS process. Circle = shallow donor, square = electron trap, and *e* = free electron. (a) An applied reverse bias results in a depletion region with no free electrons. (b) The reverse bias is increased, causing the depletion region to widen. The electron traps hold on to their electrons. (c) After some time, the electron traps have released their electrons. This results in a decrease in depletion width.

bias has swept electrons out of the depletion region, resulting in positive donors and unoccupied traps [Fig. 13(a)]. Suddenly, the reverse bias is increased, sweeping out more electrons and widening the depletion region [Fig. 13(b)]. The electron traps hold on to their electrons. As time goes on, electron traps release the electrons. This causes the positive space charge density to increase, which shrinks the depletion region. After a while, the depletion width reaches a steady-state value [Fig. 13(c)].

The depletion region plays the role of an insulating dielectric in a planar capacitor. Its width is inversely proportional to the capacitance. Therefore, the capacitance provides a convenient measure of the depletion width. By measuring the capacitive transient as a function of temperature, one can estimate the position of the deep level relative to the CBM. The deeper the level, the slower the defect will release its carrier.

DLTS and hybrid calculations indicated that Fe prefers the Ga (II) site and has a deep acceptor level 0.8 eV below the CBM.[83] This acceptor (0/−) level is also denoted as Fe^{3+}/Fe^{2+}, since Fe^{3+} is neutral relative to the Ga^{3+} host whereas Fe^{2+} is negative. EPR measurements can detect the Fe^{3+} signal. Bhandari *et al.*[84] used EPR to observe the photoexcitation of an electron from Fe^{2+} to the CB, leaving behind Fe^{3+}.
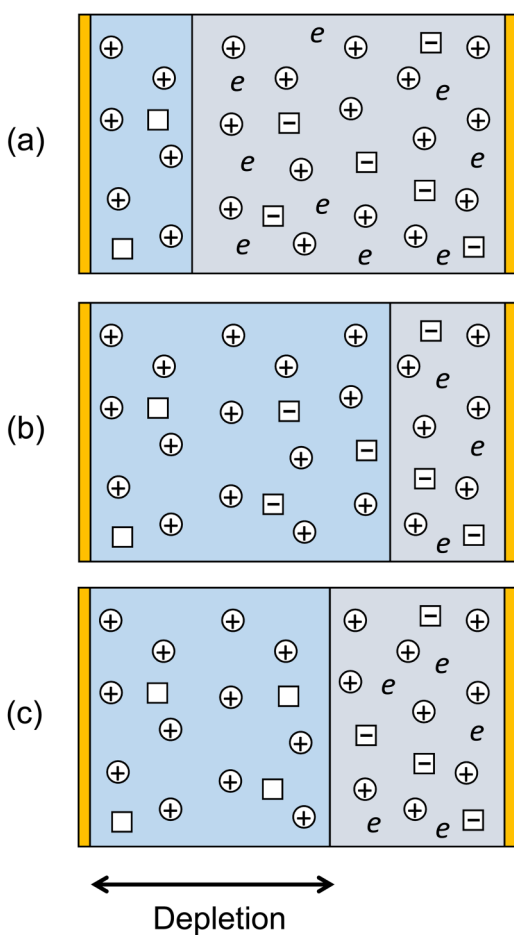
C. Iridium impurities

Bulk Ga_2O_3 crystals are commonly grown in an iridium crucible, which leads to Ir impurity incorporation in the 10^{17}–10^{18} cm^{-3} range.[79,85] Ir sits preferentially on the Ga(II) site and acts as a deep donor. In an *n*-type material, the donor is neutral. Following the convention for transition metals, this charge state is denoted as Ir^{3+}. In Mg-doped samples, Ir gives its electron to compensate the Mg acceptor, becoming positively charged (Ir^{4+}). The Ir^{4+} impurity has an IR absorption peak at 5148 cm^{-1} due to the transition of an electron from its ground state to an excited *d* orbital (Fig. 14).[79] When a sample was annealed in hydrogen, Mg acceptors became passivated (Sec. IV B) and could not accept electrons from Ir^{3+}. This led to a decrease in the 5148 cm^{-1} peak. The peak shows strong anisotropy, being weakest when the IR light is polarized along the **c** axis.[85,86]
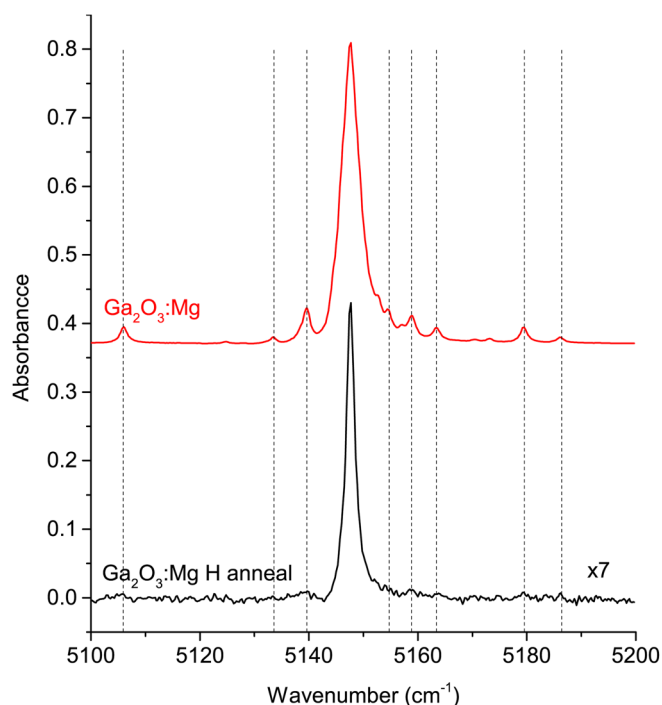
Ir^{3+} does not have a spectral signature in the IR. When a lightly *n*-type sample was illuminated with photon energies above 2.2–2.3 eV, electrons were excited from Ir^{3+} into the CB, resulting in Ir^{4+}. This caused the 5148 cm^{-1} peak to appear.[86] The threshold for this process suggests that the donor level is ~2.25 eV below the CBM, in agreement with hybrid functional calculations.

In addition to the main Ir^{4+} peak at 5148 cm^{-1}, Ritter *et al.*[86] observed numerous smaller sideband peaks in the spectral neighborhood. Because they only were observed in the Mg-doped material, these small peaks were attributed to IrMg pairs. The IrMg peaks decreased in intensity when illuminated by photons >2.2 eV. The authors suggested that this effect may be due to a photo-induced electron transfer from Mg to Ir ($Ir^{4+}Mg^- \rightarrow Ir^{3+}Mg^0$).

N-type, bulk Ga_2O_3 samples that were annealed in hydrogen show IR absorption peaks at 3313, 3437, 3450, and 3500 cm^{-1}.[79] Annealing in deuterium yields peaks that have the appropriate frequency shift. As noted in Sec. III C, the 3437 cm^{-1} peak is due to a $V_{Ga}2H$ complex. The other three peaks, however, have not been

FIG. 14. IR spectra of Mg-doped gallium oxide, as-grown and hydrogen-annealed. The peak at 5148 cm^{-1} is due to Ir^{4+}, and the sidebands are attributed to IrMg pairs. The hydrogen-annealed sample is scaled for comparison. Spectra are offset for clarity. Reprinted with permission from Ritter et al., J. Appl. Phys. **126**, 225705 (2019). Copyright 2019 AIP Publishing.[86]

identified. Ritter et al.[86] suggested that they could arise from IrH complexes. However, this assignment is tentative.

V. LUMINESCENCE

Photoluminescence (PL) spectroscopy is a sensitive technique for detecting optically active defects. In a PL experiment, an excitation light source shines on the sample. The source is often a laser but can also be light from a lamp that passes through a filter or monochromator. If the photons are above the bandgap, then electrons can be excited into the CB, leaving holes in the VB. Another way to generate electrons and holes is through electron irradiation; this is called *cathodoluminescence* (CL). In Ga$_2$O$_3$, holes form *self-trapped hole* (STH) states, which means that the hole is localized on an oxygen atom.[56,87,88] This is in contrast to electrons in the CB, which are delocalized and are free to roam. The system can return to the ground state by radiative or nonradiative paths; the radiative ones give rise to luminescence.

PL and CL spectra of Ga$_2$O$_3$ generally show broad peaks that fall into rough categories: UV, UV′, blue, and green (Fig. 15).[89] The UV band (photon energy 3.4 eV, wavelength 360 nm) is due to the recombination of an electron with an STH. This is an intrinsic feature and is not due to defects. The UV′ (3.1 eV, 400 nm) and blue bands (2.9 eV, 430 nm) have been attributed to *donor–acceptor pair* (DAP) transitions.[90,91] A DAP transition occurs when a photoexcited electron is captured by a donor and a hole is captured by an acceptor. Then, the electron tunnels from the donor to the acceptor, emitting a photon to conserve energy. Because the blue band seems to correlate with oxygen-vacancy concentration, the donor in this process was tentatively assigned to V_O.[92,93] The green band (2.4 eV, 520 nm) has also been assigned to a DAP, although
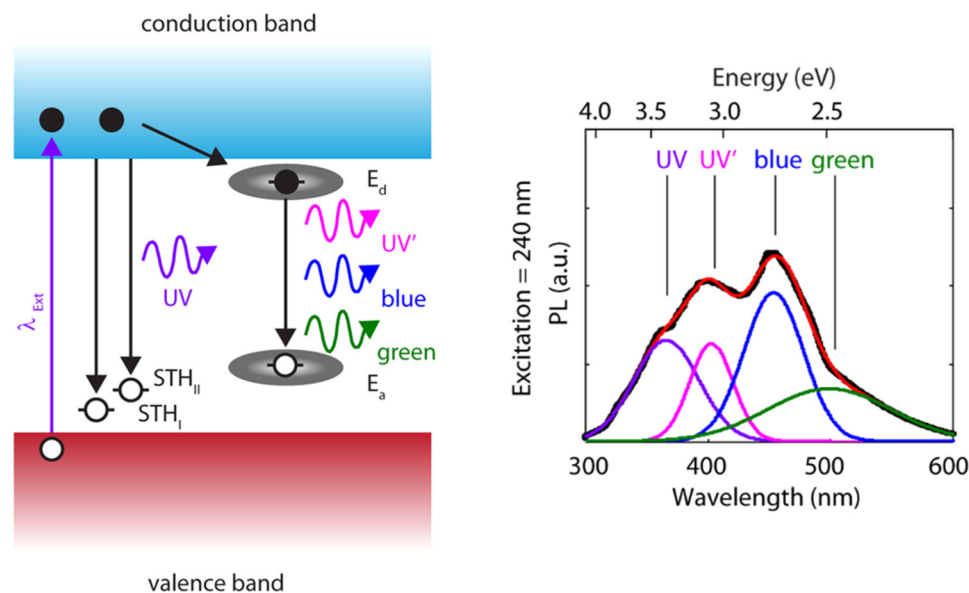
FIG. 15. Left: Energy-level diagram, where λ_{Ext} is the excitation photon, STH$_I$ and STH$_{II}$ are self-trapped hole states localized on O(I) and O(II), and a DAP transition is indicated. Right: PL spectrum showing the UV, UV′, blue, and green bands. Reprinted with permission from Wang et al., Sci. Rep. **8**, 18075 (2018). Copyright 2018 Springer Nature.[89]

there is no donor assignment. Villora *et al.*[94] noted that high O_2 pressure during growth increases the green PL intensity.

CL peaks were observed at 2.5 and 3.0 eV (500 nm and 410 nm), which are similar to the aforementioned green and blue bands. These peaks increase after neutron irradiation, suggesting that they involve V_{Ga}.[95] Chromium (Cr^{3+}) has absorption and emission spectra similar to ruby, with R_1 and R_2 lines near 1.8 eV (700 nm).[96] PL in a similar deep-red spectral range has been attributed to a transition from the CB (or shallow donor level) to the nitrogen acceptor level.[97]

VI. DAMAGE

Experiments by Ernest Rutherford's research group established the existence of the atomic nucleus when some helium ions traveling through the gold foil were observed to undergo large-angle scattering. The elastic collisions between helium and gold nuclei are analogous to collisions between billiard balls. If the kinetic energy of an energetic particle is large enough, it can knock the host atom out of its substitutional site. The rate at which defects are created is given by

$$N = \eta\phi, \tag{9}$$

where N is the defect density (cm^{-3}), η is the defect production rate (cm^{-1}), and ϕ is the particle dose (cm^{-2}).

In Ga_2O_3, gallium vacancies are deep acceptors while oxygen vacancies are deep donors. The creation of gallium vacancies in an *n*-type material causes electrical compensation that decreases the free-carrier density. Often it is the free-electron removal rate that is measured in Eq. (9), which is proportional to the number of acceptor defects that are produced. Widegap materials such as Ga_2O_3 tend to be "radiation hard," meaning the defect production rate is low.[98] This is a useful property for applications in harsh environments such as space.

One way to determine the effect of energetic particles is to place the sample in a nuclear reactor, which has fast neutrons in the 1 eV–20 MeV energy range. Such an experiment was performed on EFG-grown Ga_2O_3. The fast neutrons created deep electron traps with levels 1.3 and 2.0 eV below the CBM (determined by DLTS) with defect production rates of 8–10 cm^{-1}.[99] The generation of these traps results in a decrease in the free-electron concentration, i.e., the traps are compensating acceptor defects. Irradiation with 1.5 MeV electrons also leads to the creation of defects and reduction of carriers, with a carrier removal rate of 5 cm^{-1}.[100] Pearton *et al.*[101] compared carrier removal rates in GaN and Ga_2O_3 and found them to be roughly similar.

Implantation with 0.6 and 1.9 MeV protons results in a strong decrease in free-electron concentration for doses above 6×10^{12} cm^{-2}.[102] The free carriers are basically gone for doses above 2×10^{13} cm^{-2}. The authors attributed this to the creation of native defects such as vacancies (V_{Ga}) that compensate the donors. Thermally annealing the sample leads to a recovery of carriers, which may involve passivation by the implanted protons. EPR results combined with calculations[103] indicate that a center created by proton implantation is consistent with V_{Ga} (Sec. III B); a second center was unidentified.

VII. CONCLUSIONS

The development of Ga_2O_3 for power electronic applications requires knowledge of, and control over, point defects. Oxygen vacancies, once thought to be responsible for unintentional *n*-type conductivity, are actually deep donors. Gallium vacancies are deep acceptors that can form complexes with hydrogen. Group IV elements (Si, Ge, and Sn) and hydrogen are shallow donors, while Mg and Ca are deep acceptors with levels 1.0–1.5 eV above the VBM. The fact that acceptors are deep—along with the formation of self-trapped holes—implies that *p*-type conductivity is out of reach. However, devices utilizing semi-insulating substrates are viable.

Irradiation with energetic particles results in deep levels that have only been partially characterized. Future research may provide assignments for "unknown" defects and elucidate the role of omnipresent impurities such as C, H, and Fe. In particular, the identity of the specific donors and acceptors involved in DAP transitions has yet to be determined. Deep acceptors such as Zn have not been investigated thoroughly and may provide better characteristics than Mg or Ca. Understanding the isoelectronic center Al will be crucial for developing $(Ga_{1-x}Al_x)_2O_3$ alloys. Transition metals and other impurities introduced during growth need to be characterized.

Thus far, the majority of characterization studies on Ga_2O_3 have obtained spatially averaged quantities. Optical techniques such as CL and micro-PL have the potential to reveal inhomogeneous defect distributions with micrometer spatial resolution, while STEM can provide atomic-scale detail. For example, luminescence centers may localize at defects such as dislocations or stacking faults. High-resolution imaging of such defects will provide feedback to crystal growers and potentially identify defects that limit the critical breakdown field.

REFERENCES

[1]M. Higashiwaki, K. Sasaki, A. Kuramata, T. Masui, and S. Yamakoshi, Phys. Status Solidi A **211**, 21 (2014).

[2]S. I. Stepanov, V. I. Nikolaev, V. E. Bougrov, and A. E. Romanov, Rev. Adv. Mater. Sci. **44**, 63 (2016).

[3]S. J. Pearton, J. C. Yang, P. H. Cary, F. Ren, J. Kim, M. J. Tadjer, and M. A. Mastro, Appl. Phys. Rev. **5**, 011301 (2018).

[4]S. J. Pearton, F. Ren, M. Tadjer, and J. Kim, J. Appl. Phys. **124**, 220901 (2018).

[5]Z. Galazka, Semicond. Sci. Technol. **33**, 113001 (2018).

[6]*Gallium Oxide Technology, Devices, and Applications*, edited by S. Pearton, F. Ren, and M. Mastro (Elsevier, Amsterdam, 2019).

[7]J. Y. Tsao, S. Chowdhury, M. A. Hollis, D. Jena, N. M. Johnson, K. A. Jones, R. J. Kaplar, S. Rajan, C. G. Van de Walle, E. Bellotti, C. L. Chua, R. Collazo, M. E. Coltrin, J. A. Cooper, K. R. Evans, S. Graham, T. A. Grotjohn, E. R. Heller, M. Higashiwaki, M. S. Islam, P. W. Juodawlkis, M. A. Khan, A. D. Koehler, J. H. Leach, U. K. Mishra, R. J. Nemanich, R. C. N. Pilawa-Podgurski,

J. B. Shealy, Z. Sitar, M. J. Tadjer, A. F. Witulski, M. Wraback, and J. A. Simmons, Adv. Electron. Mater. **4**, 1600501 (2018).

[8]H. F. Mohamed, C. T. Xia, Q. L. Sai, H. Y. Cui, M. Y. Pan, and H. J. Qi, J. Semicond. **40**, 011801 (2019).

[9]A. K. Saikumar, S. D. Nehate, and K. B. Sundaram, ECS J. Solid State Sci. Technol. **8**, Q3064 (2019).

[10]B. Fu, Z. T. Jia, W. X. Mu, Y. R. Yin, J. Zhang, and X. T. Tao, J. Semicond. **40**, 011804 (2019).

[11]M. J. Tadjer, J. L. Lyons, N. Nepal, J. A. Freitas, A. D. Koehler, and G. M. Foster, ECS J. Solid State Sci. Technol. **8**, Q3187 (2019).

[12]J. J. Xu, W. Zheng, and F. Huang, J. Mater. Chem. C **7**, 8753 (2019).

[13]M. D. McCluskey and E. E. Haller, *Dopants and Defects in Semiconductors*, 2nd ed. (CRC Press, 2018).

[14]F. Tuomisto, *Characterisation and Control of Defects in Semiconductors* (IET, 2019).

[15]N. N. Greenwood and A. Earnshaw, *Chemistry of the Elements*, 2nd ed. (Butterworth-Heinemann, 1997), ISBN: 978-0-08-037941-8.

[16]M. D. McCluskey and E. E. Haller, *Dopants and Defects in Semiconductors*, 2nd ed. (CRC Press, Boca Raton, FL, 2018).

[17]M. Riorden and L. Hoddeson, *Crystal Fire*: *The Birth of the Information Age* (W.W. Norton, New York, 1997).

[18]C. T. Sah, Proc. IEEE **76**, 1280 (1988).

[19]P. J. Wellmann, Z. Anorg. Allg. Chem. **643**, 1312 (2017).

[20]M. Higashiwaki, K. Sasaki, A. Kuramata, M. Takekazu, and S. Yamakoshi, Appl. Phys. Lett. **100**, 013504 (2012).

[21]S. M. Sze and K. K. Ng, *Physics of Semiconductor Devices*, 3rd ed. (John Wiley & Sons, NJ, 2007).

[22]J. L. Hudgins, G. S. Simin, E. Santi, and M. Asif Khan, IEEE Trans. Power Electron. **18**(3), 907 (2003).

[23]A. J. Green, K. D. Chabak, E. R. Heller, R. C. Fitch, Jr., M. Baldini, A. Fiedler, K. Irmscher, G. Wagner, Z. Galazka, S. E. Tetlak, A. Crespo, K. Leedy, and G. H. Jessen, IEEE Electron. Device Lett. **37**(7), 902 (2016).

[24]B. J. Baliga, J. Appl. Phys. **53**, 1759 (1982).

[25]B. J. Baliga, IEEE Electron Device Lett. **10**(10), 455 (1989).

[26]T. Oishi, Y. Koga, K. Harada, and M. Kasu, Appl. Phys. Express **8**, 031101 (2015).

[27]S. Geller, J. Chem. Phys. **33**, 676 (1960).

[28]J. Ahman, G. Svensson, and J. Albertsson, Acta Cryst. C **52**, 1336 (1996).

[29]H. Y. He, R. Orlando, M. A. Blanco, R. Pandey, E. Amzallag, I. Baraille, and M. Rérat, Phys. Rev. B **74**, 195123 (2006).

[30]H. Peelaers and C. G. Van de Walle, Phys. Status Solidi B **252**, 828 (2015).

[31]A. Ratnaparkhe and W. R. L. Lambrecht, Appl. Phys. Lett. **110**, 132103 (2017).

[32]T.-C. Wei, D.-S. Tsai, P. Ravadgar, J.-J. Ke, M.-L. Tsai, D.-H. Lien, C.-Y. Huang, R. H. Horng, and J.-H. He, IEEE J. Sel. Top. Quant. Electron. **20**, 3802006 (2014).

[33]T. Onuma, S. Saito, K. Sasaki, T. Masui, T. Yamaguchi, T. Honda, and M. Higashiwaki, Jpn. J. Appl. Phys. **54**, 112601 (2015).

[34]M. Yamaga, T. Ishikawa, M. Yoshida, T. Hasegawa, E. G. Villora, and K. Shimamura, Phys. Status Solidi C **8**, 2621 (2011).

[35]K. Yamaguchi, Solid State Commun. **131**, 739 (2004).

[36]N. Ueda, H. Hosono, R. Waseda, and H. Kawazoe, Appl. Phys. Lett. **71**, 933 (1997).

[37]A. Mock, R. Korlacki, C. Briley, V. Darakchieva, B. Monemar, Y. Kumagai, K. Goto, M. Higashiwaki, and M. Schubert, Phys. Rev. B **96**, 245205 (2017).

[38]M. Fleischer and H. Meixner, J. Appl. Phys. **74**, 300 (1993).

[39]K. Irmscher, Z. Galazka, M. Pietsch, R. Uecker, and R. Fornari, J. Appl. Phys. **110**, 063720 (2011).

[40]N. Ma, N. Tanen, A. Verma, Z. Guo, T. Luo, H. Xing, and D. Jena, Appl. Phys. Lett. **109**, 212101 (2016).

[41]Y. Kang, K. Krishnaswamy, H. Peelaers, and C. G. Van de Walle, J. Phys. Condens. Matter. **29**, 234001 (2017).

[42]H. Peelaers and C. G. Van de Walle, Appl. Phys. Lett. **111**, 182104 (2017).

[43]Z. Galazka, R. Uecker, D. Klimm, K. Irmscher, M. Naumann, M. Pietsch, A. Kwasniewski, R. Bertram, S. Ganschow, and M. Bickermann, ECS J. Solid State Sci. Technol. **6**, Q3007 (2017).

[44]H. Aida, K. Nishiguchi, H. Takeda, N. Aota, K. Sunakawa, and Y. Yaguchi, Jpn. J. Appl. Phys. **47**, 8506 (2008).

[45]K. Hoshikawa, E. Ohba, T. Kobayashi, J. Yanagisawa, C. Miyagawa, and Y. Nakamura, J. Cryst. Growth **447**, 36 (2016).

[46]E. G. Villora, K. Shimamura, Y. Yoshikawa, K. Aoki, and N. Ichinose, J. Cryst. Growth **270**, 420 (2004).

[47]F. B. Zhang, K. Saito, T. Tanaka, M. Nishio, and Q. X. Guo, J. Cryst. Growth **387**, 96 (2014).

[48]D. W. Pashley, in *Growth and Characterisation of Semiconductors*, edited by R. A. Stradling and P. C. Klipstein (Adam Hilger, New York, 1990), pp. 1–16.

[49]Y. Yao, S. Okur, L. A. M. Lyle, G. S. Tompa, T. Salagaj, N. Sbrockey, R. F. Davis, and L. M. Porter, Mater. Res. Lett. **6**, 268 (2018).

[50]X. Xiu, L. Zhang, Y. Li, Z. Xiong, R. Zhang, and Y. Zheng, J. Semicond. **40**, 011805 (2019).

[51]E. G. Villora, K. Shimamura, K. Kitamura, and K. Aoki, Appl. Phys. Lett. **88**, 031105 (2006).

[52]K. Sasaki, A. Kuramata, T. Masui, and E. G. Villora, Appl. Phys. Express **5**, 035502 (2012).

[53]O. Ueda, N. Ikenaga, K. Koshi, K. Iizuka, A. Kuramata, K. Hanada, T. Moribayashi, S. Yamakoshi, and M. Kasu, Jpn. J. Appl. Phys. **55**, 1202BD (2016).

[54]H. Yamaguchi and A. Kuramata, J. Appl. Crystallogr. **51**, 1372 (2018).

[55]J. M. Johnson, S. Krishnamoorthy, S. Rajan, and J. Hwang, Proc. Microsc. Microanal. **23**, 1454 (2017).

[56]P. Deák, Q. D. Ho, F. Seemann, B. Aradi, M. Lorke, and T. Fraunheim, Phys. Rev. B **95**, 075208 (2017).

[57]J. B. Varley, J. R. Weber, A. Janotti, and C. G. Van de Walle, Appl. Phys. Lett. **97**, 142106 (2010).

[58]J. B. Varley, H. Peelaers, A. Janotti, and C. G. Van de Walle, J. Phys. Condens. Matter **23**, 334212 (2011).

[59]A. Kyrtsos, M. Matsubara, and E. Bellotti, Phys. Rev. B **95**, 245202 (2017).

[60]J. M. Johnson, Z. Chen, J. B. Varley, C. M. Jackson, E. Farzana, Z. Zhang, A. R. Arehart, H.-L. Huang, A. Genc, S. A. Ringel, C. G. Van de Walle, D. A. Muller, and J. Hwang, Phys. Rev. X **9**, 041027 (2019).

[61]B. E. Kananen, L. E. Halliburton, K. T. Stevens, G. K. Foundos, and N. C. Giles, Appl. Phys. Lett. **110**, 202104 (2017).

[62]F. Tuomisto and I. Makkonen, Rev. Mod. Phys. **85**, 1583 (2013).

[63]E. Korhonen, F. Tuomisto, D. Gogova, G. Wagner, M. Baldini, Z. Galazka, R. Schewski, and M. Albrecht, Appl. Phys. Lett. **106**, 242103 (2015).

[64]P. Weiser, M. Stavola, W. B. Fowler, Y. Qin, and S. Pearton, Appl. Phys. Lett. **112**, 232104 (2018).

[65]N. H. Nickel, F. Lang, E. G. Villora, K. Shimamura, and J. Rappich, AIP Adv. **9**, 105026 (2019).

[66]A. Fiedler, R. Schewski, Z. Galazka, and K. Irmscher, ECS J. Solid State Sci. Technol. **8**, Q3083 (2019).

[67]N. C. Giles and L. E. Halliburton, in *Gallium Oxide Technology, Devices, and Applications*, edited by S. Pearton, F. Ren, and M. Mastro (Elsevier, Amsterdam, 2019), Chap. 8.

[68]N. T. Son, K. Goto, K. Nomura, Q. T. Thieu, R. Togashi, H. Murakami, Y. Kumagai, A. Kuramata, M. Higashiwaki, A. Koukitu, S. Yamakoshi, B. Monemar, and E. Janzén, J. Appl. Phys. **120**, 235703 (2016).

[69]E. G. Víllora, K. Shimamura, Y. Yoshikawa, T. Ujiie, and K. Aoki, Appl. Phys. Lett. **92**, 202120 (2008).

[70]S. Mueller, H. von Wenckstern, D. Splith, F. Schmidt, and M. Grundmann, Phys. Status Solidi A **211**, 34 (2014).

[71]K. Sasaki, M. Higashiwaki, A. Kuramata, T. Masui, and S. Yamakoshi, Appl. Phys. Express **6**, 086502 (2013).

[72]S.-H. Han, A. Mauze, E. Ahmadi, T. Mates, Y. Oshima, and J. S. Speck, Semicond. Sci. Technol. **33**, 045001 (2018).

[73] A. Y. Polyakov, N. B. Smirnov, I. V. Shchemerov, D. Gogova, S. A. Tarelkin, and S. J. Pearton, J. Appl. Phys. **123**, 115702 (2018).

[74] M. Saleh, A. Bhattacharyya, J. B. Varley, S. Swain, J. Jesenovec, S. Krishnamoorthy, and K. Lynn, Appl. Phys. Express **8**, 085502 (2019).

[75] Y. Qin, M. Stavola, W. B. Fowler, P. Weiser, and S. J. Pearton, ECS J. Solid State Sci. Technol. **8**, Q3103 (2019).

[76] Z. Galazka, K. Irmscher, R. Uecker, R. Bertram, M. Pietsch, A. Kwasniewski, M. Naumann, T. Schulz, R. Schewski, D. Klimm, and M. Bickermann, J. Cryst. Growth **404**, 184 (2014).

[77] M. H. Wong, C.-H. Lin, A. Kuramata, S. Yamakoshi, H. Murakami, Y. Kumagai, and M. Higashiwaki, Appl. Phys. Lett. **113**, 102103 (2018).

[78] J. L. Lyons, Semicond. Sci. Technol. **33**, 05LT02 (2018).

[79] J. R. Ritter, J. Huso, P. T. Dickens, J. B. Varley, K. G. Lynn, and M. D. McCluskey, Appl. Phys. Lett. **113**, 052101 (2018).

[80] B. E. Kananen, L. E. Halliburton, E. M. Scherrer, K. T. Stevens, G. K. Foundos, K. B. Chang, and N. C. Giles, Appl. Phys. Lett. **111**, 072102 (2017).

[81] A. Kyrtsos, M. Matsubara, and E. Bellotti, Appl. Phys. Lett. **112**, 032108 (2018).

[82] J. R. Ritter, K. G. Lynn, and M. D. McCluskey, Proc. SPIE **10919**, 109190Z (2019).

[83] M. E. Ingebrigtsen, J. B. Varley, A. Y. Kuznetsov, B. G. Svensson, G. Alfieri, A. Mihaila, U. Badstubner, and L. Vines, Appl. Phys. Lett. **112**, 042104 (2018).

[84] S. Bhandari, M. E. Zvanut, and J. B. Varley, J. Appl. Phys. **126**, 165703 (2019).

[85] C. A. Lenyk, N. C. Giles, E. M. Scherrer, B. E. Kananen, L. E. Halliburton, K. T. Stevens, G. K. Foundos, J. D. Blevins, D. L. Dorsey, and S. Mou, J. Appl. Phys. **125**, 045703 (2019).

[86] J. R. Ritter, K. G. Lynn, and M. D. McCluskey, "Iridium-related complexes in Czochralski-grown β-Ga₂O₃," J. Appl. Phys. **126**, 225705 (2019).

[87] J. B. Varley, A. Janotti, C. Franchini, and C. G. Van de Walle, Phys. Rev. B **85**, 081109(R) (2012).

[88] B. E. Kananen, N. C. Giles, L. E. Halliburton, G. K. Foundos, K. B. Chang, and K. T. Stevens, J. Appl. Phys. **122**, 215703 (2017).

[89] Y. S. Wang, P. T. Dickens, J. B. Varley, X. Ni, E. Lotubai, S. Sprawls, F. Liu, V. Lordi, S. Krishnamoorthy, S. Blair, K. G. Lynn, M. Scarpulla, and B. Sensale-Rodriguez, Sci. Rep. **8**, 18075 (2018).

[90] L. Binet and D. Gourier, J. Phys. Chem. Solids **59**, 1241 (1998).

[91] T. T. Huynh, L. L. C. Lem, A. Kuramata, M. R. Phillips, and C. Ton-That, Phys. Rev. Mater. **2**, 105203 (2018).

[92] T. Onuma, S. Fujioka, T. Yamaguchi, M. Higashiwaki, K. Sasaki, T. Masui, and T. Honda, Appl. Phys. Lett. **103**, 041910 (2013).

[93] T. Onuma, Y. Nakata, K. Sasaki, T. Masui, T. Yamaguchi, T. Honda, A. Kuramata, S. Yamakoshi, and M. Higashiwaki, J. Appl. Phys. **124**, 075103 (2018).

[94] E. G. Villora, M. Yamaga, T. Inoue, S. Yabasi, Y. Masui, T. Sugawara, and T. Fukuda, Jpn. J. Appl. Phys. Part 2 **41**, L622 (2002).

[95] H. T. Gao, S. Muralidharan, N. Pronin, M. R. Karim, S. M. White, T. Asel, G. Foster, S. Krishnamoorthy, S. Rajan, L. R. Cao, M. Higashiwaki, H. von Wenckstern, M. Grundmann, H. Zhao, D. C. Look, and L. J. Brillson, Appl. Phys. Lett. **112**, 242102 (2018).

[96] H. H. Tippins, Phys. Rev. **137**, A865 (1965).

[97] Q. D. Ho, T. Frauenheim, and P. Deák, Phys. Rev. B **97**, 115163 (2018).

[98] J. Kim, S. J. Pearton, C. Fares, J. C. Yang, F. Ren, S. Kim, and A. Y. Polyakov, J. Mater. Chem. C **7**, 10 (2019).

[99] E. Farzana, M. F. Chaiken, T. E. Blue, A. R. Arehart, and S. A. Ringel, APL Mater. **7**, 022502 (2019).

[100] J. Yang, F. Ren, S. J. Pearton, G. Yang, J. Kim, and A. Kuramata, J. Vac. Sci. Technol. B **35**, 031208 (2017).

[101] S. Pearton, J. Yang, P. H. Cary IV, F. Ren, J. Kim, S. Pearton, F. Ren, and M. Mastro, in *Gallium Oxide Technology, Devices, and Applications* (Elsevier, Amsterdam, 2019), Chap. 14.

[102] M. E. Ingebrigtsen, A. Y. Kuznetsov, B. G. Svensson, G. Alfieri, A. Mihaila, U. Badstubner, A. Perron, L. Vines, and J. B. Varley, APL Mater. **7**, 022510 (2019).

[103] H. J. von Bardeleben, S. Q. Zhou, U. Gerstmann, D. Skachkov, W. R. L. Lambrecht, Q. D. Ho, and P. Deák, APL Mater. **7**, 022521 (2019).